Parameter Identification for Pattern-Generating Reaction-Diffusion Systems – Towards Generative Texture Descriptors

Werner Ainhauser
Bürgerstraße 32
6020 Innsbruck, Austria
werner.ainhauser98@gmail.com

Martin Welk
UMIT TIROL – Private University for
Health Sciences and Health Technology
Eduard-Wallnöfer-Zentrum 1
6060 Hall in Tirol, Austria
martin.welk@umit-tirol.at

Abstract

Spontaneous formation of patterns by reaction–diffusion systems has been a long-standing object of research. We consider an approach to utilize these systems in the processing of textured images. To this end we investigate the estimation of parameters of a pattern–generating reaction–diffusion system of Gray–Scott type from a single pattern representing the steady state distribution of one reactant. Thereby we are able to describe a texture, albeit from a limited class so far, by a set of numerical parameters. Unlike existing quantitative texture descriptors, these parameters allow reconstruction of a visually similar texture. We demonstrate our approach on synthetic and real-world textures. We consider this as a first step towards a novel class of generative texture descriptors capable of closing the loop between texture analysis and synthesis. We are convinced that with further generalizations such generative texture descriptors will become a new powerful tool for the processing of textured images.

1 Introduction

Texture analysis, such as discrimination or classification of textures [18], or segmentation of images into regions of homogeneous texture [37], is typically addressed by quantitative texture descriptors for which numerous variants have been proposed in literature over the last half century, see [4, 17, 19] for comparisons. For example, Haralick features [14, 15] use statistics of cooccurence matrices of pixel intensities. Further proposals are based on statistics of Fourier [26], Gabor [31] or wavelet coefficients [8, 25]. More recently, CNN-based descriptors have been introduced [4, 5, 13, 24]. By and large, the theoretical foundation of these approaches is mostly heuristic, and more notably, none of them allows to reconstruct the actual texture from the quantitative descriptors. Therefore, texture synthesis is done by entirely different approaches, with patch-based synthesis [9] being a prominent example. As a consequence, texture analysis and synthesis are difficult to combine, e.g. in order to design compression algorithms for textured images.

Devising a set of *generative* texture descriptors, i.e. descriptors that would allow to reconstruct the actual texture, would close the loop between texture analysis and synthesis, and therefore open avenues to novel methods in texture compression and more general texture processing. The present work is intended as a first step towards this goal. Our approach arises from the confluence of the long-researched topic of pattern formation by reaction–diffusion systems with more recent developments in parameter identification. Let us sketch these two fields shortly.

The First Austrian Symposium on AI, Robotics, and Vision (AIROV24).

Reaction–diffusion patterns The mechanism of pattern formation by reactions between (at least) two reactants (*morphogens*) combined with spatial diffusion of both substances was discovered by Alan Turing [38]. Later on, Turing patterns were identified in a wide range of chemical, physical and biological systems [2, 23], and modeled by reaction–diffusion PDEs such as the Gierer–Meinhardt [11], the Gray–Scott [12], or the Schnakenberg model [33], The root of pattern formation in these systems is the diffusion-driven instability (type I Turing instability) which means that a stable dynamical system modeling the reaction dynamics (interactions of morphogens) in a single location is driven to instability by the influence of diffusion of the reactants. Applications to the processing of textured images were envisioned in the 1990s [29, 30, 39, 40] but due to the difficulties in identifying parameters for given patterns further work was done mainly in computer graphics whereas in image analysis interest in the topic somewhat petered out.

Parameter identification Estimation of unknown parameters of a reaction–diffusion system has been considered in literature [6, 10, 16, 20, 21, 22, 35] for different scenarios. In [16], time series data are used as an input. In [20], a reaction term is estimated from initial and boundary data and a system state. In [22] a neural network is trained to estimate parameters for a pattern. Most interesting for us are [10, 35] because they follow a model-based approach and use a system state as input. To best of our knowledge, no attempt has been made so far to place the problem in the context of texture analysis. Regarding description of textures by parameter sets we mention [27] which uses neural networks trained to texture samples, thus describing textures by several thousand parameters instead of the few of a reaction–diffusion system as we intend.

Our contribution As a first step towards using parameters of reaction–diffusion systems to describe textures, we devise a workflow to estimate reaction parameters for one particular type of reaction–diffusion system (Gray–Scott) from patterns. By experiments we demonstrate the viability of the approach, albeit for the time being restricted to a limited class of textures.

Structure of the paper After recalling basics of pattern formation by reaction–diffusion systems in Section 2, the framework for parameter identification is developed in Section 3. Experiments to demonstrate the viability of our approach on synthetic and real-world examples are shown in Section 4. A short summary and outlook in Section 5 concludes the paper.

2 Pattern formation by reaction–diffusion systems

From the several reaction–diffusion models capable of generating patterns we pick the Gray-Scott model [12] for our study. It is given by an initial-value problem with suitable boundary conditions (e.g. homogeneous Neumann) for the system of coupled PDEs

$$\frac{\mathrm{d}u_1}{\mathrm{d}t} = D_1 \boldsymbol{\nabla}^2 u_1 - R u_1 u_2^2 + F(1-u_1)\,, \qquad \frac{\mathrm{d}u_2}{\mathrm{d}t} = D_2 \boldsymbol{\nabla}^2 u_2 + R u_1 u_2^2 - (F+K) u_2 \tag{1}$$

on $\Omega \times [0,T]$ where Ω is some planar domain, $[0,T]$ a time interval, and the functions $u_1, u_2 : \Omega \times [0,T] \to \mathbb{R}_+$ model concentrations of two reactants A, B that diffuse at rates D_1, D_2 within Ω and react with one another via $\mathrm{A} + 2\,\mathrm{B} \to 3\,\mathrm{B}$ with a reaction rate $R > 0$, leading to the net terms $\mp R u_1 u_2^2$ according to the mass–action law. The parameter $F > 0$, called feed rate, describes a continual renewal of the reactants by replacing a certain part of the mixture per time unit with fresh substance A, and the kill rate $K > 0$ corresponds to a process that continually removes some fraction of substance B. As usual the first morphogen is considered as the visible part of the system state. Figure 1 shows exemplary patterns generated by this system with different parameters.

Turing instability A reaction–diffusion system can be written as $\mathrm{d}\boldsymbol{u}/\mathrm{d}t = \boldsymbol{D}\boldsymbol{\nabla}^2\boldsymbol{u} + \boldsymbol{f}(\boldsymbol{u})$ where $\boldsymbol{u}$ is the vector of morphogen concentration functions, $\boldsymbol{D}$ denotes the diagonal matrix of diffusivities for the morphogens, and $\boldsymbol{f}$ comprises the reaction terms, including the feed and kill terms in the case of the example system (1). Without diffusion, $\boldsymbol{D} = \boldsymbol{0}$, a spatially constant system state $\boldsymbol{u}^*$ is stable if it is a fixed point, $(\mathrm{d}\boldsymbol{u}/\mathrm{d}t)(\boldsymbol{u}^*) = \boldsymbol{0}$, and all eigenvalues of the Jacobian $\mathrm{D}_{\boldsymbol{u}}\boldsymbol{f}$ at $\boldsymbol{u}^*$ have negative real parts. With nonzero diffusion, assuming the steady state is perturbed by a harmonic spatial wave with wave number q, the Jacobian is perturbed by $-q^2\boldsymbol{D}$ since a harmonic wave is an eigenfunction of $\boldsymbol{\nabla}^2$ with eigenvalue $-q^2$. Depending on q, the real parts of some eigenvalues of $\mathrm{D}_{\boldsymbol{u}}\boldsymbol{f} - q^2\boldsymbol{D}$ may become positive, thus creating instability. If a given system is stable without diffusion but instable

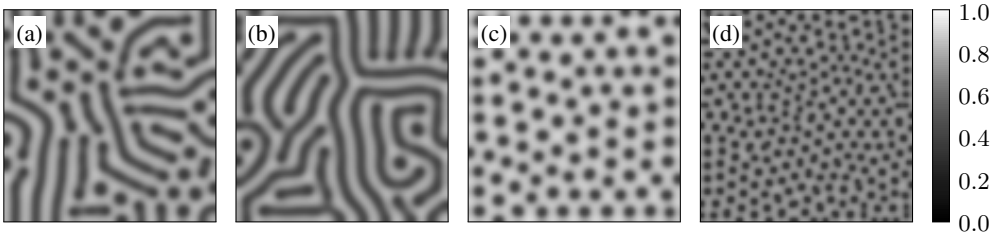

Figure 1: Four patterns (100×100 pixels each) generated by a Gray–Scott reaction–diffusion system. The concentration of the first morphogen is shown. **(a)** $D_1 = 960$, $D_2 = 360$, $F = 180$, $K = 360$, $R = 6000$. **(b)** $D_1 = 960$, $D_2 = 360$, $F = 180$, $K = 350$, $R = 6000$. **(c)** $D_1 = 960$, $D_2 = 360$, $F = 225$, $K = 400$, $R = 6000$. **(d)** $D_1 = 1000$, $D_2 = 200$, $F = 225$, $K = 400$, $R = 6000$.

for some range of wave numbers, with a maximum real part of eigenvalues being attained at some finite wave number q, the system displays a *type I Turing instability.* If instead the supremum of real parts of eigenvalues is reached for $q \to \infty$, one speaks of a *type II Turing instability.* As analyzed in literature [30, 35], type I Turing instability is the decisive mechanism behind pattern formation in a wide range of reaction–diffusion systems.

3 Parameter estimation

In order to use reaction–diffusion systems to describe textures, we pursue the goal to identify a model from an input image showing a homogeneous piece of texture. The model should be capable of producing a Turing pattern which is visually similar to the given texture. As suggested in literature [6, 10, 21] the input image is considered as a steady state of the reaction–diffusion system.

As mentioned in the previous section, reaction–diffusion systems generate Turing patterns due to the interaction of two (or more) morphogens. However, the input image represents only the concentrations of a single morphogen in the steady state. It is therefore necessary to estimate in a first step the complete steady state of the system, i.e. to complement the given image by the concentration map of the second morphogen. Once this has been accomplished, the second step involves the determination of the parameters of the reaction–diffusion system from the full steady state. The following two subsections discuss these two steps for the Gray–Scott system (1).

3.1 Estimation of the steady state

In order to estimate the missing second morphogen from the given input image, it needs to be noted that the system state at a single time t does not contain information on the dynamics of the underlying reaction–diffusion system. The question is whether the model (1) can be solved for u_2 or whether a suitable cost function can be derived from it that respects the system dynamics.

The assumption that the given image represents the morphogen u_1 in the steady state leads to the equilibrium condition

$$\frac{\mathrm{d}u_1}{\mathrm{d}t} = \frac{\mathrm{d}u_2}{\mathrm{d}t} = 0 \,. \tag{2}$$

Enforcing the steady-state constraint, the Gray–Scott system simplifies to

$$D_1 \boldsymbol{\nabla}^2 u_1 - R u_1 u_2^2 + F(1 - u_1) = 0 \,, \qquad D_2 \boldsymbol{\nabla}^2 u_2 + R u_1 u_2^2 - (F + K) u_2 = 0 \,. \tag{3}$$

We assume for now that the parameters of the Gray–Scott system are known.

Polynomial fitting Numerical experiments with the Gray–Scott system with different parameters lead to the observation that there is a strong negative correlation between the concentrations of the morphogen u_1 and u_2 across the spatial domain, compare Figure 2(a) (ground truth for one example run of (1)). This is also in accordance with the understanding of the dynamical system as an activation–inhibition mechanism that suggests a complementary distribution of the two morphogens.

This inspires to use a linear model $u_2 = f(u_1, \boldsymbol{c}) = c_1 u + c_0$ with coefficients $\boldsymbol{c} = (c_0, c_1)$ still to be specified. Unfortunately, since only u_1 is known, linear regression cannot be used to fit the

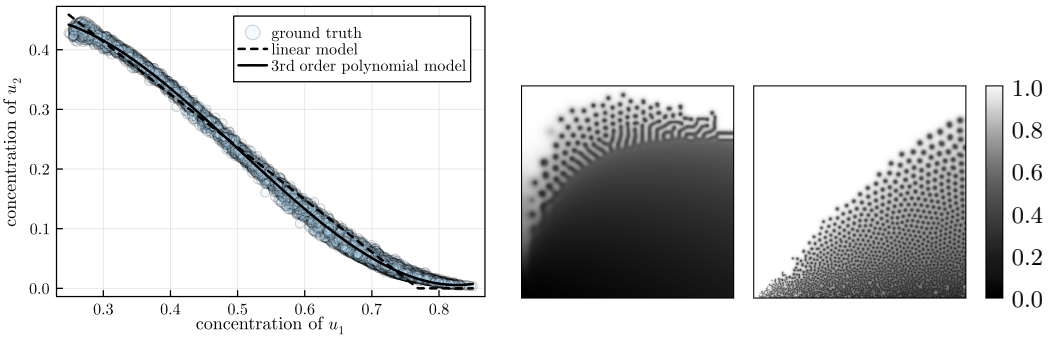

(a) (b) (c)

Figure 2: **(a)** Phase diagram of the reference system compared to a linear model and a third-order polynomial model. Negative values are clipped. **(b, c)** Parameter maps obtained by running (1) with spatially varying parameters. In (b) the diffusion rates were fixed, feed rate increasing from 0 (left) to 800 (right), kill rate from 0 (bottom) to 800 (top), reaction rate $R = 10^4$. In (c) F, K, R were fixed, and D_1 varied from 0 (left) to 1500 (right), D_2 from 0 (bottom) to 800 (top).

coefficients. Based on (2), we introduce the cost function

$$J_{\mathrm{I}}(\boldsymbol{c}) = \sum_p \left(\left(\frac{\mathrm{d}u_1(p)}{\mathrm{d}t} \right)^2 + \left(\frac{\mathrm{d}u_2(p)}{\mathrm{d}t} \right)^2 \right) \tag{4}$$

where p runs over pixels, u_2 is computed pixel-wise from u_1 via the linear model with c_0, c_1, and the derivatives $\mathrm{d}u_i/\mathrm{d}t$ are given by (1). The cost function can be interpreted as a distance to the equilibrium of (1). Starting from some initialization, c_0, c_1 can now be refined iteratively using a gradient descent for J_{I}, leading to a minimizer $\boldsymbol{c}_{\mathrm{lin}} = (c_0, c_1)$ for J_{I}.

As shown in Figure 2(a), the correlation between the morphogens is well captured by the fitted linear model. For a better fit, the linear model can be replaced by a cubic polynomial $u_2 = P(u_1, \boldsymbol{c}) = c_3 u_1^3 + c_2 u_1^2 + c_1 u_1 + c_0$. As before, a minimizer $\boldsymbol{c}_{\mathrm{cub}} = (c_0, c_1, c_2, c_3)$ can be estimated by gradient descent for $J_{\mathrm{I}}(\boldsymbol{c})$, and yields an even better approximation of the correspondence between the morphogens, see again Figure 2(a). Note that unnatural negative concentrations of u_2 for high u_1 can occur, especially with the linear model, which need to be clipped for proper functioning of (1).

Direct optimization As an alternative to the polynomial fitting approach,it is also possible to estimate $\boldsymbol{u}_2$ directly by gradient descent for J_{I}. To this end, (1) is substituted for $\mathrm{d}u_k/\mathrm{d}t$ in J_{I}, and the Laplacians $\boldsymbol{\nabla} u_{k;i,j}$ at pixels $p = (i, j)$ are expressed by a standard central-difference discretization $\boldsymbol{\nabla} u_{k;i,j} = u_{k;i+1,j} + u_{k;i-1,j} + u_{k;i,j+1} + u_{k;i,j-1} - 4\, u_{k;i,j}$ to yield J_{I} as a function of the $u_{2;i,j}$. The derivatives $\mathrm{d}J_{\mathrm{I}}/\mathrm{d}u_{2;i,j}$ can then be computed either by numerical differentiation or by automatic differentiation in reverse mode [3]. In experiments, this approach yields a slightly more accurate reconstruction of u_2 than the polynomial fitting approach but at a substantially higher computational expense (more than three orders of magnitude). For the rest of this paper, we settle therefore for the cubic polynomial fitting approach.

3.2 Estimation of the parameters of the PDE system

We turn now to discuss how, given a full steady state of a Gray–Scott system, the parameters can be estimated. Numerical experiments have shown that the reaction parameters are relevant for the type of texture generated by the system, whereas the diffusion rates essentially determine the scaling, compare Figure 1. One can therefore choose between a computationally cheaper estimation of the reaction parameters only, with fixed diffusivities, or full estimation of reaction and diffusion parameters. The proceeding is analogous in both cases.

Pattern formation capability Turing instability occurs only in certain regions of the parameter space, Figure 2(b, c). For a given system state consisting of morphogen concentration maps on Ω, we

say that the system with given parameters has *pattern formation capability* if at least one point in Ω satisfies the criterion of a type I Turing instability.

We use this criterion to constrain the feasible region in the parameter space. For its evaluation, we employ an adapted version of an algorithm from [35] that samples a range of wave numbers with logarithmic spacing and analyses for each pixel in Ω the eigenvalues of the system for all sample wave numbers. A pixel is classified as type I Turing instability if the real part of the largest real part of an eigenvalue is positive for some wave number and descends again towards the highest wave number. Note that the pattern formation capability is a necessary but not a sufficient criterion.

Simplifying an approach from [10], we test whether the given system state is a steady state for the reaction–diffusion system with given parameters by simulating the system for one time step, and evaluating the resulting updates to the morphogen concentrations. From these updates, a cost function is constructed which is then minimized.

We consider four choices of the cost function. The simplest choice is J_{I} from (4) in the previous subsection. Its gradient w.r.t. the system parameters can be evaluated by automatic differentiation and used for a gradient descent step for these parameters. An alternative that captures more of the non-linear behavior of the system evolution is

$$J_{\mathrm{II}} = \sum_{p} \left(\tilde{\boldsymbol{u}}(p) - \boldsymbol{u}(p)\right)^2 \tag{5}$$

where $\boldsymbol{u}$ and $\tilde{\boldsymbol{u}}$ denote the given state and the state after a prescribed short evolution time (amounting to several simulated time steps), resp., and summation again runs over all pixels p in Ω. The gradient of J_{II} is computed numerically by simulating the system for the current and nearby parameters.

Whereas the cost function J_{II} measures the discrepancy between $\boldsymbol{u}$ and $\tilde{\boldsymbol{u}}$ directly in terms of morphogen concentrations, the comparison can be focused stronger on properties of textures by measuring discrepancies of suitable texture features. We consider two choices of texture features: HGM (histogram of gradient magnitudes) descriptors [36] and ORB (Oriented FAST and Rotated BRIEF) features [32]. HGM analyzes the distribution of gradients within an image, binning them according to their magnitude. We normalize the gradient magnitudes to $[0, 1]$ to compensate for contrast and fix the number of bins to 20. The L^1 norm of the difference of the resulting normalized HGM of $\boldsymbol{u}$ and $\tilde{\boldsymbol{u}}$ yields the cost function J_{III}. ORB identifies corner-like key points in images and equips them with a descriptor based on an orientation-normalized neighborhood patch. The descriptor is a binary string encoding intensity comparisons within the patch. Thus, the discrepancy of ORB between $\boldsymbol{u}$ and $\tilde{\boldsymbol{u}}$ is measured by the Hamming distance of the descriptors of a fixed number (here, 10) of best-matched features in both images (from a total of 1000 key points computed per image). The resulting cost function is J_{IV}. Since both J_{III} and J_{IV} take discrete values due to their construction from histograms and Hamming distances, resp., they require gradient-free optimization; we use the Nelder–Mead algorithm [28] for this purpose.

3.3 Alternating estimation of the steady state and PDE parameters

The proposed method of finding model parameters from an image only is illustrated in Figure 3. For simplicity, we assume here that only reaction parameters are estimated. An image and a reaction–diffusion model with known diffusivities are thus required as inputs. Further, a start value must be provided for the reaction parameters $\boldsymbol{\theta}_0$. An upper and lower bound is provided for each parameter θ_k in $\boldsymbol{\theta}$. Within the so specified parameter range, suitable initializations for the reaction parameters are identified based the pattern capability criterion from Section 3.2. To this end, random samples $\boldsymbol{\theta}$ are drawn uniformly distributed on the parameter range. For each sample $\boldsymbol{\theta}$ the full concentration state of the reaction–diffusion system is estimated by polynomial fitting as described in Section 3.1, and the pattern formation capability is evaluated on the estimated system state. The process is repeated until a desired number of valid initial parameter sets are found. The parameter set $\boldsymbol{\theta}_0$ with the lowest cost is then used as the initial value for parameter optimization.

Parameter optimization proceeds by alternating between updating the parameter set $\boldsymbol{\theta}_i$ and the system state estimate. The parameter update is performed by non-linear optimization using one of the cost functions functions J_{I} to J_{IV} using Nelder–Mead optimization consistently. The result of the optimization are new reaction parameters $\boldsymbol{\theta}_{i+1}$ with a lower cost. The alternating update process of parameters and system state stops if the cost function converges to a (local) minimum yielding optimal parameters $\boldsymbol{\theta}_{\mathrm{opt}}$, or after a maximum number of iterations.

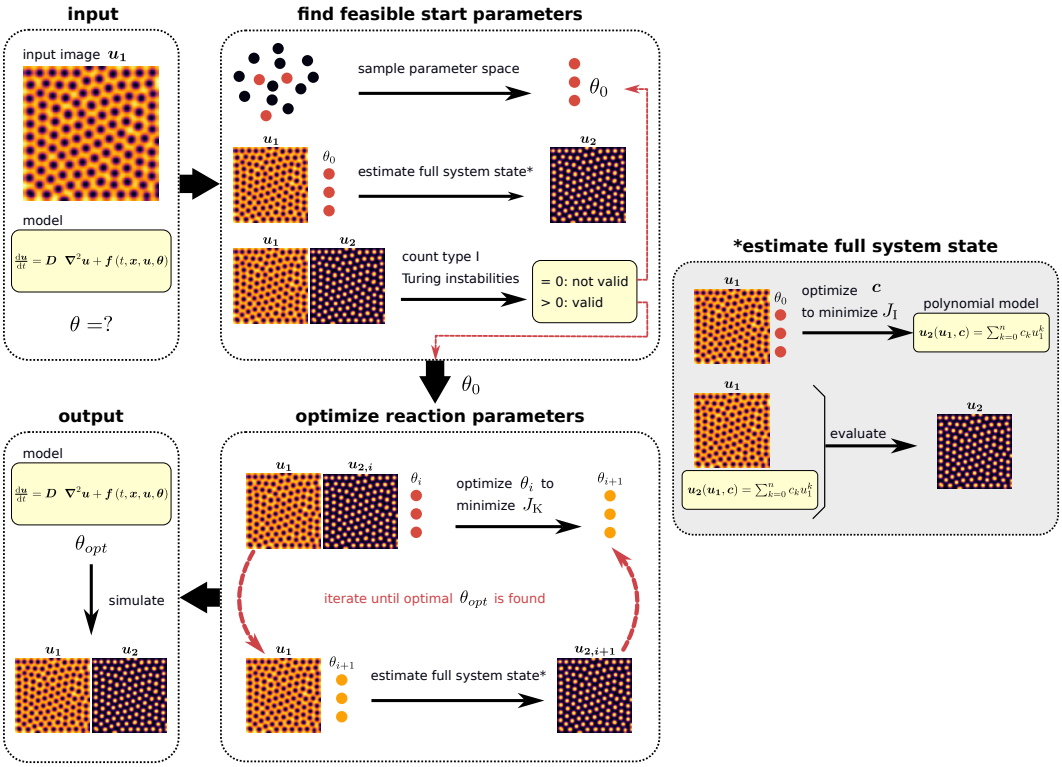

Figure 3: Workflow to estimate reaction parameters of a reaction–diffusion model from pattern data.

3.4 Texture reconstruction

After successful estimation of the parameters of the reaction–diffusion system, one is interested in reconstructing a pattern from these parameters. To this end, however, the system state must be initialized suitably. The unknown initialization is a common problem in the literature [10, 21, 34]. In some applications it can be assumed that initial conditions are known, but not for texture synthesis, since in general, we want to approximate textures that originally were not generated by a reaction–diffusion simulation. In our simulations, we initialize the morphogen concentrations by random values uniformly distributed in intervals given by the ranges observed in the equilibrium state.

4 Experiments

For experiments, our method was implemented in Julia 1.8.2. On a recent PC, single-core CPU computation times for parameter estimation from 100×100 pixel test images ranged from approx. 15 s with cost function J_I to approx. 900 s with J_IV. Algorithmic optimizations and potential GPU implementation are expected to reduce computation times significantly but are left for future work.

4.1 Synthetic patterns

In our first experiment, Figure 4, we use our model with the four different cost functions to estimate parameters for a pattern (frame a) that has been generated by the Gray–Scott system so we can compare the estimated parameters to the known ground truth, and visually assess the texture similarity. In this experiment, we estimate only reaction parameters while keeping the diffusion parameters fixed. We start with a setting in which the diffusion rates and reaction parameters were chosen close to the ground truth (frames b–e). Next we perturb the input image with moderate Gaussian noise (frame f) and try to estimate system parameters from the noise input image. Returning to the noise-free input image, we test the ability of the method to find correct parameters from an initialization farther away from the ground truth (frames k–n) and with wrong assumptions on the diffusion rates (frames o–r).

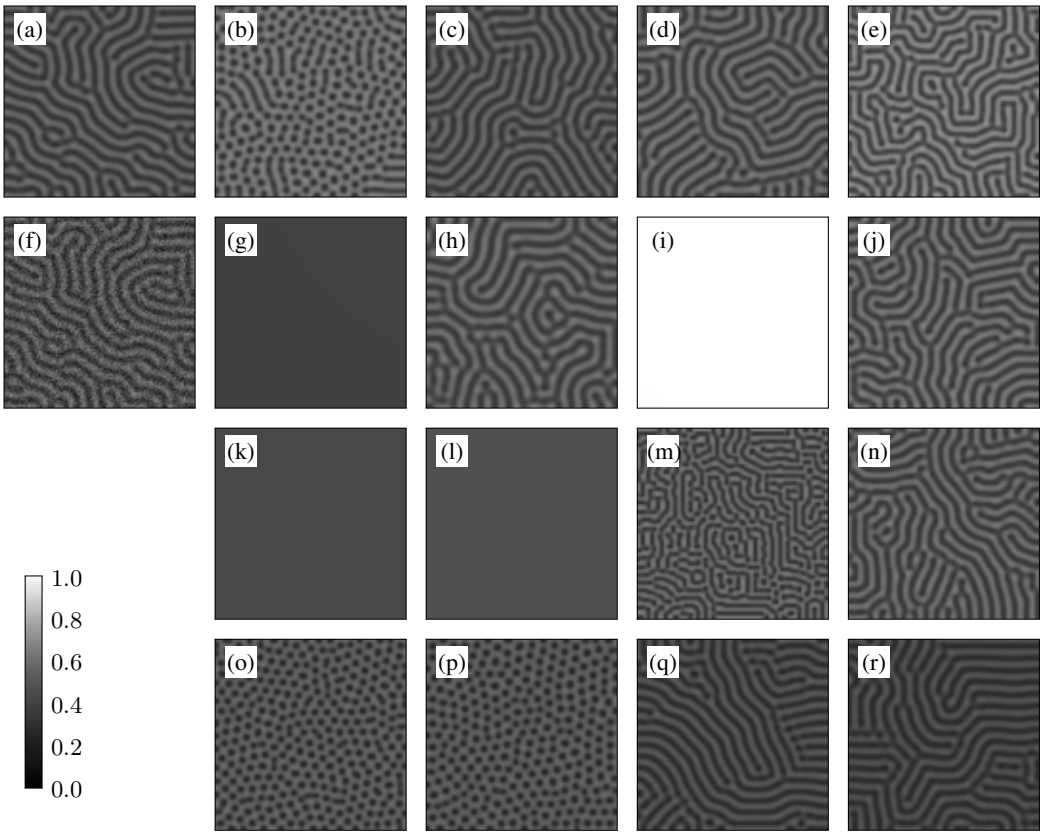

Figure 4: Experiments with synthetic pattern. Parameter values are available as supplemental material. **(a)** Pattern generated by Gray–Scott system. **(b–e)** Patterns synthesized after parameter estimation from image (a) where correct diffusion rates and reaction parameters close to the ground truth were used for initialization, and cost functions J_{I} (b), J_{II} (c), J_{III} (d) and J_{IV} (e) used in the optimization. **(f)** Pattern from (a) degraded by Gaussian noise, standard deviation 0.05. **(g–j)** Patterns synthesized after parameter estimation from image (f), same parameters as in (b–e). **(k–n)** Same as (b–e) but reaction parameters initialized farther away from the ground truth. **(o–r)** Same as (b–e) but with fixed diffusion rates chosen lower than the ground-truth values.

Estimation with the gradient-based cost function J_{I} (frames b, g, k, o) fails to reconstruct the proper type of texture, and yields no texture at all under noise or with initialization too far from the ground truth parameters (g, k). The cost function J_{II} (frames c, h, l, p) which is based on proper system simulation and intensity measure yields a reasonable reconstruction if initialized close to the ground truth (c), even under moderate noise (h), but fails when initialized with more deviant parameters (l, p). The HGM-based J_{III} (frames d, i, m, q) leads to parameters encoding the correct pattern type in all noise-free cases (d, m, q) but fails under noise. The ORB-based cost function J_{IV} (frames e, j, n, r) succeeds in all cases. We remark that currently the method does not always cope well with initial parameters far away from correct values. Improving robustness thus remains a goal for further work.

4.2 Real-world patterns

In our second experiment, Figure 5, we explore the ability of our model to adapt to real-world textures, using examples from the Describable Texture Database [7]. Given that at the time being only the Gray–Scott system is used, we select two images that resemble the typical spot-like and stripe-like patterns generated by the Gray–Scott system, along with one that does not match either of these types precisely (scaly snake skin). Parameter estimation here involves reaction and diffusion parameters. Because of the limitations regarding initialization pointed out in 4.1, we run the estimation several times with different initializations and report the (visually) best results.

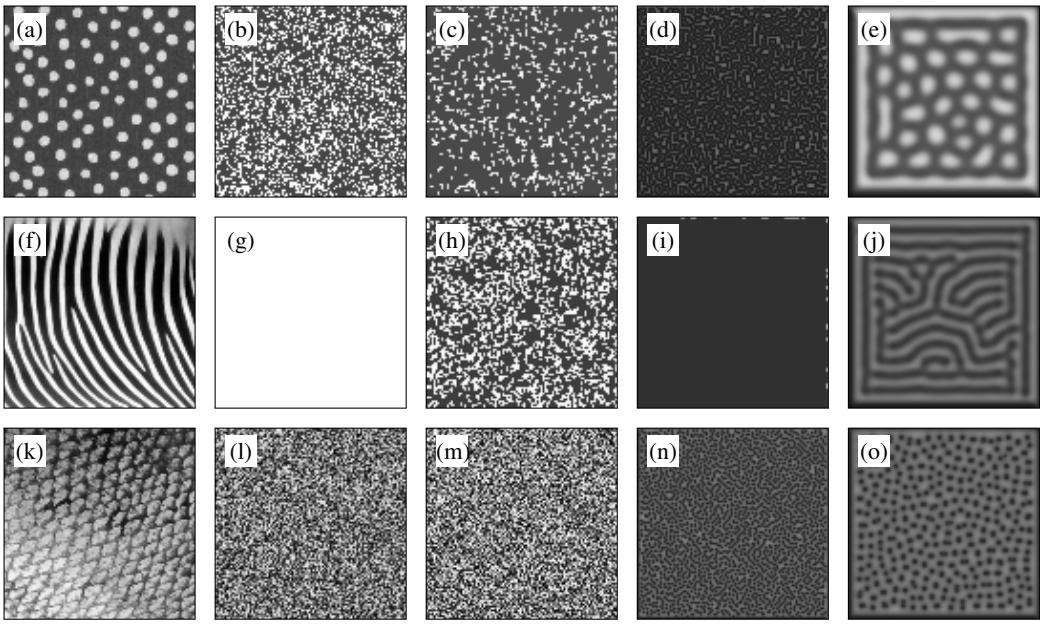

Figure 5: Experiments with real-world texture examples. Parameter values are available as supplemental material. **(a, f, k)** Input images (100×100 pixels) clipped, rescaled and converted to gray-scale from the Describable Texture Database [7], items *dotted_0202* (a), *striped_0101* (f) and *scaly_0167* (k). **(b–e, g–j, l–o)** Patterns synthesized after parameter estimation from images (a, f, k), resp., using cost functions J_{I} (b, g, l), J_{II} (c, h, m), J_{III} (d, i, n) and J_{IV} (e, j, o) in the optimization.

With cost functions J_{II} and J_{IV}, pattern-generating parameter sets are found in all cases, whereas J_{I} and J_{III} achieve this only for one and two, resp., of the textures. Only the ORB-based cost function J_{IV} succeeds in reconstructing the correct type of patterns in the spotted and striped textures. As can be expected due to the isotropic nature of the dynamical system, the preferred direction of stripes in the second example cannot be represented. For the scaly texture, cost functions J_{III} and J_{IV} find approximations by spot patterns where for J_{IV} the scale roughly matches the quasi-periodic structure.

5 Summary and conclusion

We have demonstrated in this work how reaction parameters, or reaction and diffusion parameters of a reaction–diffusion system for pattern formation can be estimated from nothing but an image representing the steady-state distribution of one morphogen. Albeit restricted for the time being to the types of patterns generated by one particular (Gray–Scott) system, this suggests that PDE parameters can be used to describe textures by quantitative descriptors from which the textures can be reconstructed. To best of our knowledge this is a novelty among quantitative texture descriptors and opens avenues to new applications in texture processing such as compression of textured images.

Of course, to bring this approach to practical texture processing contexts still needs further developments. As already mentioned this involves speeding up computations by algorithmic optimizations and GPU implementation. Regarding the method itself, modifications should be made to accommodate anisotropic features (see the stripe directions in Figure 5(f)) as well as the technicality of handling overall brightness and contrast.

On a more fundamental level, however, two main generalizations appear paramount. On one hand, it is necessary to integrate into the framework more types of pattern–forming reaction–diffusion systems along with automated selection between these systems, thus transitioning from parameter identification to system identification. On the other hand, more complex textures might not be representable by a plain reaction–diffusion system but may be decomposed into simpler components for which this is possible. We have made first steps along both directions of generalization in our ongoing work, results of which we expect to present in a forthcoming publication.

Acknowledgments

This work is based on the master thesis [1] written by the first author at UMIT TIROL within a joint degree programme of UMIT TIROL and University of Innsbruck.

References

[1] W. Ainhauser. Identification of reaction–diffusion systems from textures. Master thesis, UMIT TIROL, Hall in Tirol, Austria, 2023.

[2] J. Bard. A model for generating aspects of zebra and other mammalian coat patterns. *Journal of Theoretical Biology*, 93(2):363–385, 1981.

[3] A. G. Baydin, B. A. Pearlmutter, A. A. Radul, and J. M. Siskind. Automatic differentiation in machine learning: a survey. *Journal of Marchine Learning Research*, 18:1–43, 2018.

[4] R. Bello-Cerezo, F. Bianconi, F. Di Maria, P. Napoletano, and F. Smeraldi. Comparative evaluation of hand-crafted image descriptors vs. off-the-shelf CNN-based features for colour texture classification under ideal and realistic conditions. *Applied Sciences*, 9:738.1–32, 2019.

[5] B. Bhandari, A. Alsadoon, P. Prasad, S. Abdullah, and S. Haddad. Deep learning neural network for texture feature extraction in oral cancer: Enhanced loss function. *Multimedia Tools and Applications*, 79:27867–27890, 2020.

[6] E. Campillo-Funollet, C. Venkataraman, and A. Madzvamuse. Bayesian parameter identification for Turing systems on stationary and evolving domains. *Bulletin of Mathematical Biology*, 81:81–104, 2019.

[7] M. Cimpoi, S. Maji, I. Kokkinos, S. Mohamed, and A. Vedaldi. Describing textures in the wild. In *Proceedings of the IEEE Conference on Computer Vision and Pattern Recognition*, pages 3606–3613, 2014.

[8] Y. Dong, J. Feng, L. Liang, L. Zheng, and Q. Wu. Multiscale sampling based texture image classification. *IEEE Signal Processing Letters*, 24(5):614–618, 2017.

[9] A. A. Efros and T. K. Leung. Texture synthesis by non-parametric sampling. In *Proc. International Conference on Computer Vision (ICCV 1999)*, volume 2, pages 1033–1038, 1999.

[10] M. R. Garvie, P. K. Maini, and C. Trenchea. An efficient and robust numerical algorithm for estimating parameters in Turing systems. *Journal of Computational Physics*, 229(19):7058–7071, 2010.

[11] A. Gierer and H. Meinhardt. A theory of biological pattern formation. *Kybernetik*, 12(1):30–39, 1972.

[12] P. Gray and S. K. Scott. Autocatalytic reactions in the isothermal, continuous stirred tank reactor: Oscillations and instabilities in the system A+ 2B $\rightarrow$ 3B; B $\rightarrow$ C. *Chemical Engineering Science*, 39(6):1087–1097, 1984.

[13] D. Han, H. Nie, J. Chen, M. Chen, Z. Deng, and J. Zhang. Multi-modal haptic image recognition based on deep learning. *Sensor Review*, 2018.

[14] R. Haralick. Statistical and structural approaches to texture. *Proceedings of the IEEE*, 67(5):786–804, 1979.

[15] R. Haralick, K. Shanmugam, and I. Dinstein. Textural features for image classification. *IEEE Transactions on Systems, Man, and Cybernetics*, 3(6):610–621, 1973.

[16] M. Hoffmann, C. Fröhner, and F. Noé. Reactive SINDy: Discovering governing reactions from concentration data. *Journal of Chemical Physics*, 150(2), 2019.

[17] P. Howarth and S. Rüger. Evaluation of texture features for content-based image retrieval. In P. Enser, Y. Kompatsiaris, N. O'Connor, A. Smeaton, and A. Smeulders, editors, *Image and Video Retrieval*, volume 3115 of *Lecture Notes in Computer Science*, pages 326–334. Springer, Berlin, 2004.

[18] K. Huang and R. Murphy. Automated classification of subcellular patterns in multicell images without segmentation into single cells. In *Proc. 2004 IEEE International Symposium on Biomedical Imaging*, volume 2, pages 1139–1142, 2004.

[19] A. Humeau-Heurtier. Texture feature extraction methods: A survey. *IEEE Access*, 7:8975–9000, 2019.

[20] B. Kaltenbacher and W. Rundell. On the identification of a nonlinear term in a reaction–diffusion equation. *Inverse Problems*, 35(11):115007, 2019.

[21] A. Kazarnikov and H. Haario. Statistical approach for parameter identification by Turing patterns. *Journal of Theoretical Biology*, 501:110319, 2020.

[22] J. Kho, W. Koh, J. C. Wong, P.-H. Chiu, and C. C. OOi. Design of Turing systems with physics-informed neural networks. In H. Ishibuchi, C.-K. Kwoh, A.-H. Tan, D. Srinivasan, C. Miao, A. Trivedi, and K. Crockett, editors, *Proceedings of the 2022 IEEE Symposium Series on Computational Intelligence (SSCI 2022), 4–7 December 2022*, pages 1180–1186. IEEE, Singapore, 2022.

[23] S. Kondo and R. Asai. A reaction–diffusion wave on the skin of the marine angelfish Pomacanthus. *Nature*, 376:765–768, 1995.

[24] C. Li and Y. Huang. Deep decomposition of circularly symmetric Gabor wavelet for rotation-invariant texture image classification. In *2017 IEEE International Conference on Image Processing (ICIP)*, pages 2702–2706, 2017.

[25] S. Livens, P. Scheunders, G. van de Wouwer, and D. Van Dyck. Wavelets for texture analysis, an overview. In *1997 Sixth International Conference on Image Processing and Its Applications*, volume 2, pages 581–585. IET, 1997.

[26] R. Maani, S. Kalra, and Y.-H. Yang. Noise robust rotation invariant features for texture classification. *Pattern Recognition*, 46(8):2103–2116, 2013.

[27] A. Mordvintsev, E. Niklasson, and E. Randazzo. Texture generation with neural cellular automata. Technical Report cs.AI:2105.07299, arXiv.org, 2021.

[28] J. A. Nelder and R. Mead. A simplex method for function minimization. *The computer journal*, 7(4):308–313, 1965.

[29] C. Price, P. Wambacq, and A. Oosterlinck. Computing with reaction–diffusion systems: applications in image processing. In D. Roose, B. De Dier, and A. Spence, editors, *Continuation and Bifurcations: Numerical Techniques and Applications*, pages 379–387. Kluwer, Dordrecht, 1990.

[30] C. Price, P. Wambacq, and A. Oosterlinck. Image enhancement and analysis with reaction–diffusion paradigm. *IEE Proceedings*, 137:I(3):136–146, 1990.

[31] F. Riaz, A. Hassan, S. Rehman, and U. Qamar. Texture classification using rotation- and scale-invariant Gabor texture features. *IEEE Signal Processing Letters*, 20(6):863–870, 2013.

[32] E. Rublee, V. Rabaud, K. Konolige, and G. Bradski. ORB: an efficient alternative to SIFT or SURF. In *Proceedings of the IEEE International Conference on Computer Vision*, pages 2564–2571, 2011.

[33] J. Schnakenberg. Simple chemical reaction systems with limit cycle behaviour. *Journal of Theoretical Biology*, 81(3):389–400, 1979.

[34] D. Schnörr and C. Schnörr. Learning system parameters from Turing patterns. *arXiv preprint arXiv:2108.08542*, 2021.

[35] N. S. Scholes, D. Schnoerr, M. Isalan, and M. P. Stumpf. A comprehensive network atlas reveals that Turing patterns are common but not robust. *Cell systems*, 9(3):243–257, 2019.

[36] M. Sharma and H. Ghosh. Histogram of gradient magnitudes: a rotation invariant texture-descriptor. In *2015 IEEE International Conference on Image Processing (ICIP)*, pages 4614–4618. IEEE, 2015.

[37] L. Tesař, A. Shimizu, D. Smutek, H. Kobatake, and S. Nawano. Medical image analysis of 3D CT images based on extension of Haralick texture features. *Computerized Medical Imaging and Graphics*, 32(6):513–520, 2008.

[38] A. M. Turing. The chemical basis of morphogenesis. *Philosophical Transactions of the Royal Society (part B)*, 237:37–72, 1953.

[39] G. Turk. Generating textures on arbitrary surfaces using reaction–diffusion. In *Proceedings of ACM SIGGRAPH 91*, pages 289–298, 1991.

[40] A. Witkin and M. Kass. Reaction–diffusion textures. In *Proceedings of ACM SIGGRAPH 91*, pages 299–308, 1991.